ULTRASONIC PLATE WAVE EVALUATION OF NATURAL FIBER COMPOSITE PANELS

Brian J. Tucker†

Senior Research Scientist
Pacific Northwest National Laboratory
P.O. Box 999 MS K5-26
Richland, WA 99352

Donald A. Bender†

Director and Professor
Wood Materials and Engineering Laboratory
Washington State University
Pullman, WA 99164-1806

David G. Pollock

Assistant Professor
Civil and Environmental Engineering
Washington State University
Pullman, WA 99164-2910

and

Michael P. Wolcott†

Associate Professor
Wood Materials and Engineering Laboratory
Washington State University
Pullman, WA 99164-1806

ABSTRACT

Two key shortcomings of current ultrasonic nondestructive evaluation (NDE) techniques for plywood, medium density fiberboard (MDF), and oriented strandboard are the reliance on empirical correlations and the neglect of valuable waveform information. The research reported herein examined the feasibility of using fundamental mechanics, wave propagation, and laminated, shear deformable plate theories to nondestructively evaluate material properties in natural fiber-based composite panels. Dispersion curves were constructed exhibiting the variation of flexural plate wave phase velocity with frequency. Based on shear deformable laminated plate wave theory, flexural and transverse shear rigidity values for solid transversely isotropic, laminated transversely isotropic, and solid orthotropic natural fiber-based composite panels were obtained from the dispersion curves. Axial rigidity values were obtained directly from extensional plate wave phase velocity. Excellent agreement (within 3%) of flexural rigidity values was obtained between NDE and mechanical testing for most panels. Transverse shear modulus values obtained from plate wave tests were within 4% of values obtained from through-thickness ultrasonic shear wave speed. Tensile and compressive axial rigidity values obtained from NDE were 22% to 41% higher than mechanical tension and compression test results. These differences between NDE and axial mechanical testing results are likely due to load-rate effects; however, these large differences were not apparent in the flexural and transverse shear comparisons. This fundamental research advances the state-of-the-art of NDE of wood-based composites by replac-

---

ing empirical approaches with a technique based on fundamental mechanics, shear deformation laminated plate theory, and plate wave propagation theory.

INTRODUCTION

Ultrasonic techniques have been employed in the nondestructive evaluation (NDE) of wood and wood-based composite panels because they are easily integrated with in-line production at relatively low cost. Stress wave techniques have proven useful for *in-situ* assessment of logs and standing trees (Halabe et al. 1997; Ross 1999; Ross et al. 1999). Ultrasonic techniques have proven to be effective for sorting and grading of veneer (Brashaw et al. 1996). In a laboratory press, acousto-ultrasonic methods have been used to monitor the degree of resin curing in wood panel products (Beall and Chen 1997). For final product evaluation, flexural modulus of wood-based composites was closely predicted using a stress wave approach (Ross and Pellerin 1988). Acoustic emission (AE) and acousto-ultrasonics (AU) have also been used to evaluate wood-based composites such as panel and glue laminated members (Beall 1990; Beall and Biernacki 1992; Petit et al. 1992; Sato and Fushitani 1992). These techniques, while robust, often rely on empirical correlations of material properties with ultrasonic signal features such as first-arrival transit time, attenuation, and amplitude; meanwhile, additional information in the ultrasonic waveform is typically disregarded.

In this study, a fundamental examination of ultrasonic wave propagation in wood-based panels has resulted in a method to directly measure flexural *and* transverse shear properties of natural fiber composite panels without the need for empirical correlations. More accurate material property information is obtained with this method when compared to many existing ultrasonic nondestructive evaluation methods. In addition, transverse shear stiffness, a material property not previously evaluated using ultrasonic NDE, can be directly determined.

Ultrasonic plate waves have been analyzed with fundamental wave propagation and material mechanics theories to successfully examine high-modulus fiber composites for NDE techniques in the aerospace industry (Rose 1999; Tang et al. 1988; Tang and Henneke 1989). These techniques are capable of directly measuring the effective flexural and transverse shear rigidity of high-modulus laminated fiber composites. Based on the material similarities between high-modulus fiber composites and fiber-based wood composites, it is proposed that similar techniques could be applicable to NDE of natural fiber-based composites.

OBJECTIVES

In an attempt to advance the wood NDE state-of-the-art, a thorough background study of wave propagation in laminated composites was carried out, specifically in the area of plates. The goal of this research is to determine the feasibility of using flexural plate waves to assess the elastic properties of natural fiber-based composite panels. Specifically, this research is designed to:

1) Establish and verify an experimental method using plate waves to inspect natural fiber-based composite panels; and
2) Validate the ability of plate waves to predict effective axial, flexural, and transverse shear rigidities for selected pseudo-homogeneous solid and layered natural fiber-based composite panels.

BACKGROUND

What are ultrasonic plate waves?

An *ultrasonic* wave is simply a wave that propagates at a frequency above the range of human hearing (generally above 20,000 Hz). An ideal ultrasonic bulk wave is a three-di-
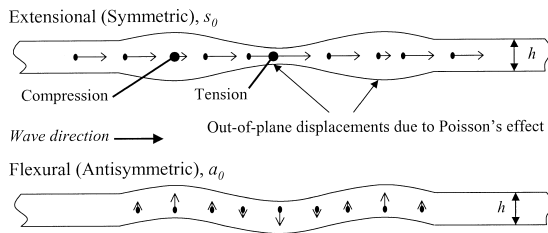
Extensional (Symmetric), s_0

Compression   Tension

Wave direction ⟶   Out-of-plane displacements due to Poisson's effect

Flexural (Antisymmetric), a_0

FIG. 1.   Displacement patterns for the lowest order extensional and flexural Lamb wave modes, s_0 and a_0 (also termed plate waves).
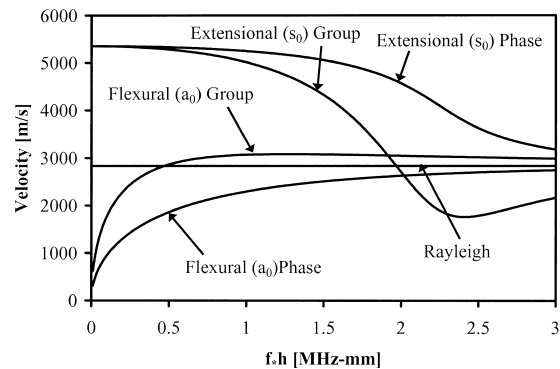

FIG. 2.   Dispersion curves for 6061-T4 aluminum plate wave modes based on elasticity theory: as $f \cdot h$ approaches zero, flexural plate wave phase velocity is greatly affected by changes in frequency and thickness; extensional phase velocity remains relatively constant at the $f \cdot h$ zero limit; all converge to Rayleigh wave speed as $f \cdot h$ values approach infinity.

mensional spherical disturbance that originates from a point source and propagates through an infinite homogeneous medium. When the infinite medium is bounded by an upper and lower surface (such as a plate with length and width dimensions much greater than the thickness), the spherical disturbance reflects back on itself within the thickness of the plate. This interference results in a dispersive wave propagation behavior known as Lamb wave propagation.

Lamb wave propagation occurs when the wavelength, λ, is between 1/10th and 10 times the plate thickness ($0.1h < \lambda < 10h$) (Bray and Stanley 1997). The remaining dimensions (length and width) of the plate must be much greater than the wavelength. Lamb waves have two distinct types of propagation discernible by their particle displacement patterns and velocities: extensional (symmetric, s) and flexural (antisymmetric, a), each of which has an infinite number of modes ($s_0, s_1, s_2, \ldots, s_n$ and $a_0, a_1, a_2, \ldots, a_n$) at higher frequencies (Auld 1973; Graff 1975; Rose 1999; Viktorov 1967). At low frequencies (typically used in NDE of wood), only the lowest order Lamb wave modes (s_0, a_0) exist. This research uses only these two fundamental Lamb wave modes, which are commonly termed plate waves.

Plate wave modes typically exhibit wavelengths much larger than the plate thickness. A simple rule-of-thumb to verify conditions for plate wave propagation is to make sure that the flexural wavelength is at least three times greater than the plate thickness ($\lambda > 3h$) and the extensional wavelength is at least five times greater than the plate thickness ($\lambda > 5h$) (Huang 1999). Because of the low frequency and long wavelength of plate waves, they "perceive" the composite and/or laminate through which they are traveling as a *solid homogeneous material* (through the thickness) (Tang et al. 1988). Based on Mindlin plate theory (Mindlin 1951), the wave characteristics depend on the *effective* material properties of the entire plate instead of discrete individual layers. The particle motion of the extensional plate mode is parallel with the direction of wave propagation, while the flexural particle motion is perpendicular to the direction of wave propagation (Fig. 1).

What is a dispersive wave?

A dispersive wave is defined as a wave whose velocity is frequency-dependent. This behavior can result from material properties (viscoelasticity) or material geometry (such as a thin plate or rod). Dispersion curves for the lowest-order flexural and extensional Lamb wave modes (Fig. 2) illustrate how phase and group velocity change as a function of the frequency-thickness ($f \cdot h$) product. Dispersion curves are generally plotted versus the $f \cdot h$ product to normalize plates of similar material
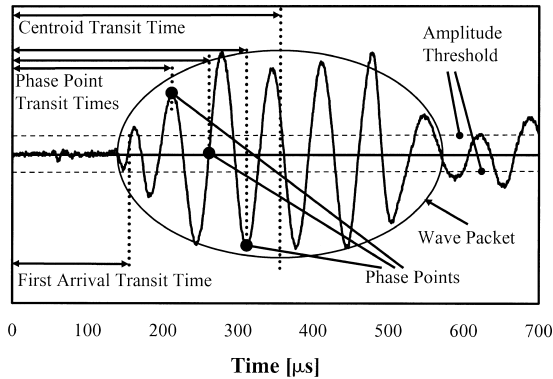
FIG. 3. Dispersive wave packet from a 15-kHz, 4-cycle sinusoidal tone burst: first arrival transit time is commonly used for current ultrasonic NDE of wood; phase point transit time is used to calculate phase velocity; centroid transit time is used to calculate group velocity.

with respect to thickness. For dispersive wave propagation (e.g., flexural plate waves, surface waves in water), group and phase velocities differ implying that the individual phase points within a wave packet (Fig. 3) will move relative to the centroid of the wave packet. This difference between phase and group velocity leads to distortion of the wave packet as it travels through a material. For nondispersive wave propagation (e.g., bulk waves in elastic materials or extensional plate waves at the zero $f \cdot h$ limit), phase velocity and group velocity are equal (Fig. 2); therefore, the wave does not distort as it propagates. As $f \cdot h$ approaches zero, extensional mode velocities remain relatively constant, whereas flexural mode velocities change rapidly. When $f \cdot h$ reaches approximately 0.5, the extensional mode velocity begins to change rapidly; however, the flexural mode velocity begins to level off. Finally, as $f \cdot h$ values approach infinity, group and phase velocity of both extensional and flexural modes converge to the Rayleigh wave speed, c_R (Rose 1999). Plate wave theory assumes that the wavelength is much larger than the panel thickness, which is generally associated with low $f \cdot h$ (below approximately 0.5) values, and as such, the extensional mode is relatively *non*dispersive and the flexural mode is highly dispersive.

What are phase and group velocity?

Historically, NDE in the wood literature has based wave speed on the transit time of the first crossing of a specified amplitude threshold in the received signal (Fig. 3). In plate wave applications, the information *following* the first arrival is generally used, which includes a wave "packet" and the specific information contained therein. Phase velocity (Eq. 1) is defined as the speed of individual, well-defined phase points (identified as the peaks, valleys, and zero crossings in a wave packet) through a material. Group velocity, defined as the speed of a wave packet through a material, is generally more difficult to measure than phase velocity due to the inaccurate determination of the wave packet centroid. Phase velocity calculations are more accurate, less ambiguous, and offer more redundant measurements (phase points) of transit time within a wave packet.

$$c_{ph} = \frac{\omega}{k} = f\lambda \qquad (1)$$

c_{ph} = phase velocity [m/s]
ω = radial propagation frequency [rad/s]
k = wave number (or wave vector) [rad/m]
f = frequency [Hz]
λ = wavelength [m]

In order to calculate phase velocities, waveforms must be captured from at least two locations of the receiving transducer along the same line of action away from the sending transducer. A more detailed description of this method is presented in the Methods section. The change in distance of the receiving transducer is divided by the change in phase point transit time to obtain phase velocity.

How are material properties determined from plate wave phase velocities?

Using basic wave propagation theory combined with Mindlin laminated plate theory (Mindlin 1951), Stiffler (1986) developed a set of governing equations (Eqs. 2–5) to describe plate wave behavior in the two global material

directions (1- and 2-directions) of a cross-ply laminated plate. As stated earlier, these equations rely on the main assumption that the wavelength is much greater than the plate thickness, which is generally the case with plate waves ($f \cdot h$ values approximately below 0.5). Other assumptions derived from lamination theory include small strains, small displacements, negligible strain through the thickness (constant thickness), transverse shear stresses vanish on top and bottom surfaces, and each layer of the laminate obeys Hooke's law. These relationships closely approximate the more computationally intensive general elasticity approach and may be used to solve for effective axial (A_{11} and A_{22}), flexural (D_{11} and D_{22}), and transverse shear (A_{55} and A_{44}) plate rigidities, which are effective elastic material properties defined in shear deformable laminated plate theory. The nondispersive (not frequency-dependent) extensional mode phase velocity allows for direct calculation of the axial plate rigidities using Eqs. (4) and (5). However, a nonlinear technique is required to fit the flexural dispersion relations (Eqs. 2 and 3) to the experimentally obtained flexural plate wave phase velocities (Huang et al. 1998). The lower portion of the flexural dispersion curve ($f \cdot h$ approaches zero) is governed by the flexural rigidity of the wave medium. As $f \cdot h$ increases, the transverse shear rigidity of the plate has a larger effect on the shape of the curve. As $f \cdot h$ approaches infinity, the phase velocity tends to approach the Rayleigh wave speed, which is solely dependent on the transverse shear modulus of the material.

Flexural 1-direction

$$(D_{11}k_1^2 + A_{55} - I\omega^2)(A_{55}k_1^2 - \bar{\rho}\omega^2) - A_{55}^2 k_1^2 = 0 \tag{2}$$

Flexural 2-direction

$$(D_{22}k_2^2 + A_{44} - I\omega^2)(A_{44}k_2^2 - \bar{\rho}\omega^2) - A_{44}^2 k_2^2 = 0 \tag{3}$$

Extensional 1-direction

$$A_{11}k_1^2 - \bar{\rho}\omega^2 = 0 \tag{4}$$

Flexural 2-direction

$$A_{22}k_2^2 - \bar{\rho}\omega^2 = 0 \tag{5}$$

where

D_{11}, D_{22} = effective laminate bending rigidities in principal directions [N-m]

A_{55}, A_{44} = effective laminate transverse shear rigidities in principal directions [N/m]

A_{11}, A_{22} = effective laminate axial rigidities in principal directions [N/m]

k_i = wave number (or wave vector) in i-direction of material [rad/m]

$\bar{\rho}$ = effective density [kg/m²]; $\bar{\rho} = \int_{-h/2}^{h/2} \rho \, dz$

I = rotational inertia term [kg]; $I = \int_{-h/2}^{h/2} \rho z^2 \, dz$

ρ = mass density [kg/m³]

z = distance from midplane of plate [m]

How are plate waves experimentally transmitted through wood panels?

The plate wave technique, also termed acousto-ultrasonic technique, was used in previous research for evaluation of carbon fiber epoxy laminates (Tang et al. 1988; Tang and Henneke 1989) by placing compression (p-wave) transducers in direct normal contact on the same side of the specimen. Ultrasonic gel couplant (similar to that used for medical ultrasound) was used between the transducers and the specimen. By exciting the sending transducer at very low frequencies (between 10 kHz and 1 MHz), plate waves were introduced into the specimen. A variation of this technique is illustrated in the Methods section.

MATERIALS

The goal of material selection was to provide plate forms of natural fiber composites with different directional properties. Specifically, thin plates measuring 610 mm square were produced in either a transversely isotro-
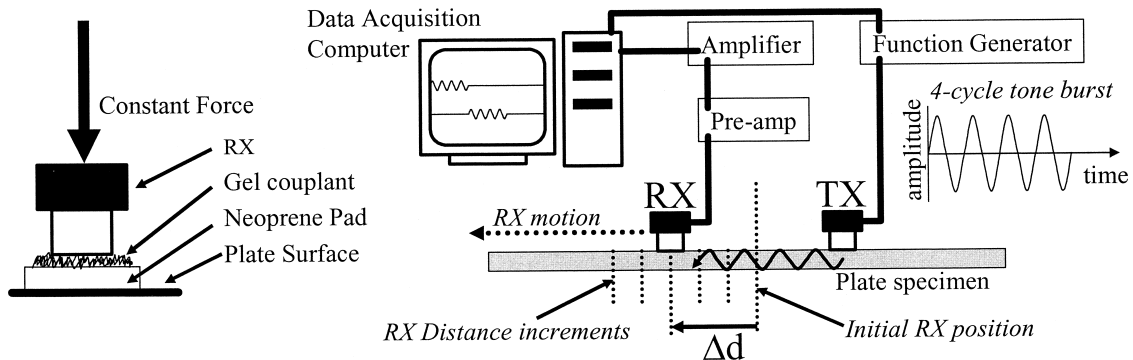
FIG. 4. Plate wave setup: TX was excited with a 4-cycle sinusoidal tone burst, RX detected the signal, which was then amplified and stored digitally; RX was then moved away from TX by a known distance and the 4-cycle burst was repeated.

pic or orthotropic form. Composites with small fiber furnishes were selected to minimize void volume and maximize material homogeneity. All panels were hand-formed and manufactured in a laboratory-scale, computer-controlled hot-press to a target density of 640 kg/m^3. Four types of plates were fabricated: 1) 3.2-mm solid transversely isotropic, 2) 6.4-mm solid transversely isotropic, 3) 6.4-mm laminated transversely isotropic, and 4) 3.2-mm orthotropic.

Six 3.2-mm and two 6.4-mm transversely isotropic plates were produced using commercial medium density fiberboard (MDF) pressure-refined wood fibers combined with 10% by weight powdered phenol-formaldehyde resin (Plenco 12631). The resinated fiber was randomly aligned parallel to the panel surface, thereby producing a single plane of isotropy within the panel. Two 3.2-mm plates were laminated with commercial polyvinyl acetate adhesive (Titebond by Franklin International) to form a 6.4-mm-thick panel. The laminate was fabricated to verify the ability of plate waves to "perceive" a layered composite as a solid material having overall effective material properties.

The orthotropic plate was produced to a thickness of 3.2 mm using wheat straw fiber (obtained from commercial straw bales), hammermilled to a length of 6.4 mm, and combined with 6% liquid polymeric methyl di-iso-cyanate (pMDI) resin (Bayer Mondur 541). The resulting straw fiber was elongated, relatively flat, and easily oriented by passing it through a 60 kV/m electric field during the forming process. This alignment produced plates with properties differing parallel and perpendicular to the aligned directions, as well as normal to the panel plane.

METHODS

Plate wave setup

Plate waves were transmitted and acquired using an experimental setup (Tucker 2001) (Fig. 4) similar to that used by Tang and Henneke (1989) and Stiffler (1986). Panametrics broadband transducers with a central frequency of 1 MHz were placed in normal contact with the specimen surface and used to transmit and receive the ultrasonic plate waves. The small contact area (approximately 198 mm^2) of the 1-MHz transducer allowed for increased signal resolution at $f \cdot h$ around 0.25 and above, but reduced sensitivity compared to larger face area (approximately 792 mm^2 and above) transducers (Huang 1998). Transducer locations used for testing are illustrated in Fig. 5. Coupling of the transducers to the specimens was achieved using Neoprene pads, ultrasonic gel, and constant contact pressure. The gel was applied only at the interface between the transducer face and the Neoprene, providing con-

sistent results on uneven surfaces without absorption of the couplant into the specimens. Plate specimens were supported on foam blocks except for a 9-cm-wide strip below the transducers (Fig. 5). This gap minimized wave energy leakage into the supports. Panel thickness was measured at RX locations (Fig. 5) and found to be within ±0.025 mm of the average thickness of all RX locations. Wave propagation was measured in only one direction for the transversely isotropic panels. Both directions, parallel (1-direction) and perpendicular (2-direction) to the fiber orientation, were tested on the orthotropic panel.

Wave excitation and reception

A Hewlett Packard 8116A function generator was used to excite the sending transducer (TX) with a 4-cycle, ±8-volt sinusoidal tone burst. The transducer vibrations created plate waves in the panel, which were detected by the receiving transducer (RX). The signal was amplified using the preamp portion of a Panametrics 5058PR pulser-receiver and was stored digitally on a computer using a Gage 2125 data acquisition card. The initial location of the receiving transducer relative to the sending transducer was approximately 10 cm center to center. RX was moved away from TX using a screw-driven Velmex™ slide with an accuracy of 1/100 mm. The increments between RX locations (Fig. 5) varied depending on frequency and wavelength. At higher frequencies (shorter wavelengths), 0.5-cm increments were used to prevent incorrect phase point selection. At lower frequencies (longer wavelengths), 2-cm increments were used to increase transit time resolution. With this transducer configuration, reflections from the plate edges were minimized; however, only the central 80-mm region of the panel was actually tested.

At the initial, intermediate, and final locations of RX, TX was excited with several discrete tone burst frequencies. Excitation frequencies from 5 to 25 kHz at 2.5-kHz increments were used to generate flexural plate
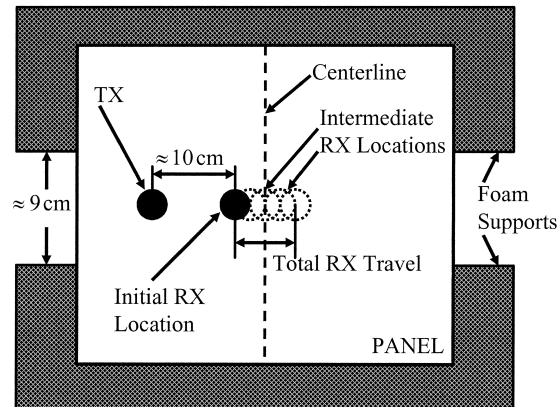

FIG. 5.   Top view of setup showing transducer locations, panel centerline, and foam supports: total RX travel and RX increments were governed by frequency; at higher frequencies, smaller RX increments were used; at lower frequencies, larger RX increments were used.

waves in the 6.4-mm panels, whereas the thinner 3.2-mm panels were tested between 5 and 50 kHz at 5-kHz increments. To generate extensional plate waves, frequencies between 35 and 60 kHz were used for 6.4-mm and between 50 and 120 kHz were used for 3.2-mm panels. Due to transducer characteristics, the actual propagated wave frequency and the excitation tone burst frequency were not always equal (Seale and Madaras 2000). Therefore, the actual propagated frequency was calculated from the period of the received signal. The frequency increments were varied to achieve the same dispersion curve resolution for panels of different thickness. Excitation frequency ranges were governed by limitations of the test equipment to accurately transmit and detect waveforms.

Signal interpretation and analysis

The test configuration used for this research excited both extensional and flexural plate waves simultaneously. The sending transducer could detect only out-of-plane displacements and could not distinguish between the two modes. Therefore, two characteristics of plate wave propagation were exploited to discriminate between the modes: 1) out-of-plane displacement magnitude changes as a function of
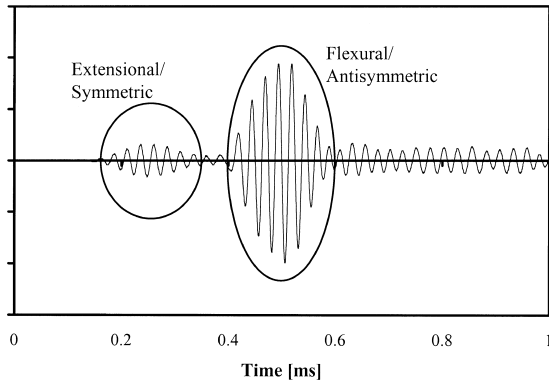
Fɪɢ. 6.   Signal excited at 80 kHz ($f \cdot h$ = 0.25 MHz-mm): faster traveling extensional wave arrived before flexural wave; this minimized interference between modes and simplified signal analysis.

$f \cdot h$ and 2) extensional and flexural waves possess different group velocities.

With the transducer placement (normal contact) used in this research, the out-of-plane displacement of the flexural mode was not only much larger in amplitude than the extensional mode, but also stayed relatively constant over the frequency range (5 to 50 kHz) used herein. The extensional plate wave was not easily detectable at low frequencies (below approximately 20 kHz) (Fig. 3) and thus the flexural mode was easily isolated and analyzed. This phenomenon of the undetectable extensional mode at low frequencies was observed by Stiffler (1986), but no explanation was given; however, Rose (1999) reports that displacement patterns change with $f \cdot h$. For the extensional modes, as $f \cdot h$ increases, the out-of-plane displacement increases, which also increases the ability to detect the mode with normal contact transducers.

At higher frequencies (approximately 20 kHz and above), the out-of-plane displacement of the extensional mode became more pronounced in the received signal, adding complexity to signal interpretation. However, since the extensional plate wave group velocity was generally much faster than the flexural wave for the frequencies used in this research (Fig. 2), a sufficient initial distance of approximately 10 cm between transducers allowed the ex-

tensional mode to arrive much earlier than the flexural mode, resulting in easy identification and separation of wave modes. Figure 6 illustrates a received signal containing both extensional and flexural modes at an excitation frequency of 80 kHz. The short duration, 4-cycle tone burst also minimized interference of the extensional mode's trailing edge with the leading edge of the flexural mode.

A Labview program (Tucker 2001) was created to calculate phase velocities at each frequency for both extensional and flexural plate wave modes. For a given frequency, up to five phase points were identified and tracked at each RX location in the received signals (Fig. 7). The relative RX distance was plotted versus the transit time of these phase points. Phase velocity was obtained from the slope of the plots. Using several phase points provided redundant phase velocity values for construction of the dispersion curve.

Calculation of plate rigidities

Dispersion curves (shown in the Results section) for the flexural waves were constructed by plotting the experimentally obtained phase velocities versus the $f \cdot h$ product. The nonlinear dispersion relation(s) (Eqs. 2 and 3) were fit to the data using the generalized reduced gradient method (GRG2), resulting in the effective flexural and transverse shear rigidities, D_{11} and A_{55} (Huang et al. 1998). Initial estimates of D_{11} and A_{55} were used to generate phase velocities coincident with $f \cdot h$ values from experimental testing. Final rigidity values were obtained by minimizing the sum of the squares of the difference between the experimental and calculated velocities. Considering D_{11} and A_{55} as variables in a 2-dimensional space (Eq. 6) where m is the number of velocity measurements at different frequencies, V^e is the experimental phase velocity and V^c is the calculated phase velocity using Eq. (2) for a given set of D_{11} and A_{55}, final rigidity values were obtained (Huang et al. 1998).
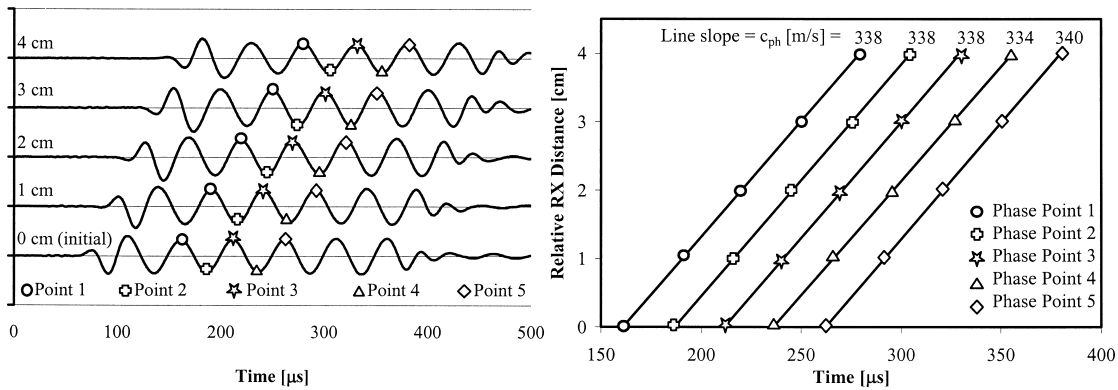
FIG. 7. At a particular frequency (20 kHz used here), phase points (peaks, valleys, or zero crossings) were followed in time (left) as RX was moved away from TX; phase velocity, c_{ph}, can be obtained from the slope of the RX distance vs. phase point time (right).

$$\min_{(D_{11}, A_{55})} \sum_{i=1}^{m} (V_i^e - V_i^c)^2 \qquad (6)$$

The robustness of the numerical solution was verified by entering a wide range of initial values, all resulting in the same end values for D_{11} and A_{55}. Axial rigidities were simply obtained directly from the average extensional mode phase velocity (Eqs. 4 and 5).

To verify the overall accuracy of the experimental apparatus and conditions, an aluminum plate specimen measuring 3.2 mm thick was tested nondestructively to determine the plate rigidities, A_{11}, D_{11}, and A_{55}. Assuming an isotropic plate using a Poisson's ratio of 0.33, Young's modulus, E, was calculated from both the axial and flexural rigidities (A_{11} and D_{11}) to within 1% of nominal values for the aluminum 6061-T4 alloy (Ensminger 1988). From the transverse shear rigidity, A_{55}, the shear modulus was calculated to within 7% of the nominal published value.

Mechanical bending setup

Three-point flexural bending tests (Fig. 8) were performed on the panels to determine the overall plate flexural rigidity. Line-load and knife edge supports were used to create a simply supported span equal to 40 times the plate thickness to minimize the effect of transverse shear deformations. The line-load and one
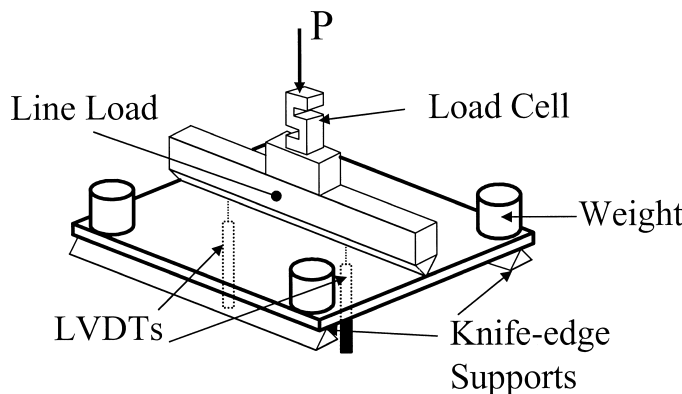

FIG. 8. Three point, simply supported bending setup: knife edge supports, line load at midspan measured with load cell, two LVDTs, and weights to counteract minor panel warp.
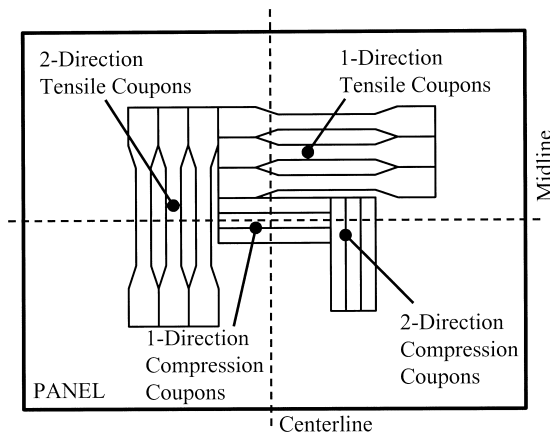
FIG. 9.   Location of axial coupons removed from panel: plate wave test area (center of panel) was not coincident with all axial coupon locations.

support were allowed to swivel perpendicular to the test span to accommodate unsymmetrical bending. Two Sensotec™ model 060-3587-04 LVDTs measured deflection at 15.25 cm from the midline of the panels to observe any unsymmetrical bending due to panel material inhomogeneities. Total centerline displace-
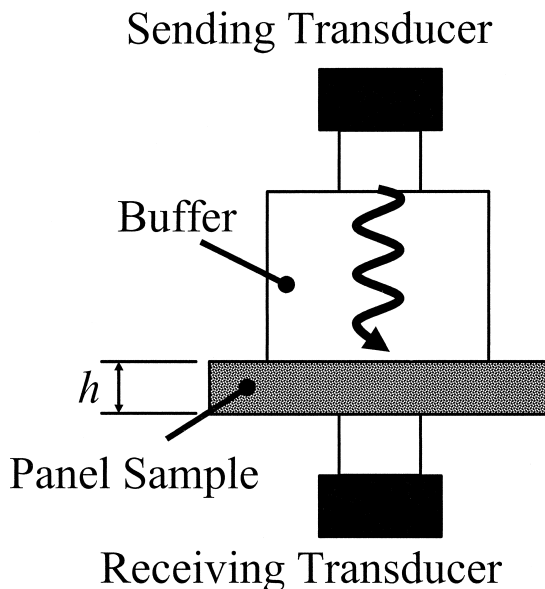

FIG. 10.   Through-thickness shear modulus setup: transit time through the sample is determined by subtracting buffer transit time from the transit time through both buffer and sample.

ment was calculated by averaging the two LVDT readings. A single 222-N capacity SSM-50 Interface load cell was used to measure the total line load on the specimen. Weights were placed on the panel edges directly above the supports to insure that contact between the panel and knife edges was maintained for slightly warped specimens. A strain rate of 1.0% per min was used to deflect the panel to a maximum strain of 0.5%. From the slope of the load-displacement curve, flexural rigidity, D_{11}, was calculated according to Eq. (7) where P is the load, d is the displacement, L is the clear span, and w is the panel width perpendicular to span.

$$D_{11} = \left(\frac{P}{d}\right)\frac{L^3}{48w} \qquad (7)$$

Axial coupon specimens

After NDE and full plate bending tests were conducted on each panel, axial testing coupons were cut from selected panels at the locations illustrated in Fig. 9. Tensile coupons were sized and tested according to ASTM D 638 (ASTM 2000) and compressive coupons were sized and tested according to ASTM D 695 (ASTM 1996). Results from the mechanical tests were compared with the NDE results to validate the applicability of the plate wave technique for measuring axial elastic panel properties.

Through-thickness ultrasonic testing

Mechanical determination of transverse shear modulus, G, for wood has historically been difficult and somewhat inaccurate. Therefore, validation of shear modulus was done ultrasonically using two 250-kHz Panametrics broadband normal incidence shear wave transducers to propagate bulk shear waves directly through the panel thickness. A similar method was used by Tauchert and Guzelsu (1972) (Fig. 10). Through-thickness determination of shear modulus uses a *bulk* shear wave, which differs greatly from the plate wave technique. The bulk shear modulus

was used for comparison with the shear modulus obtained using the plate wave technique. Transverse shear rigidity, A_{55}, the thickness, h, and the shear correction coefficient ($K = 0.833$) may be used to calculate the shear modulus (Eq. 8) (Tang et al. 1988). Only panels dissected for axial coupons were tested using shear wave NDE.

$$A_{55} = GhK \qquad (8)$$

RESULTS AND DISCUSSION

Signal analysis

For each panel, wavelength was calculated after testing to verify that the low frequency, long wavelength assumptions required for plate wave propagation were not violated. During flexural plate wave tests, the shorter wavelengths approached the $3h$ limit, but did not fall below it, indicating that the long wavelength assumption was not violated. Extensional plate waves were transmitted at higher excitation frequencies due to their small out-of-plane motion at lower frequencies (Rose 1999); however, the wavelengths did not fall below the $5h$ limit, again satisfying the plate wave assumptions.

Rose (1999) and Viktorov (1967) describe cutoff frequencies, below which higher Lamb wave modes do not propagate. After the fundamental flexural and extensional modes, the next highest Lamb wave mode to appear as $f \cdot h$ increases is the second flexural (a_1) mode. The $f \cdot h$ value at which this mode arrives is governed by the bulk transverse shear velocity ($f \cdot h = c_T/2$). The lowest bulk transverse shear velocity for all panels tested was found in the 2-direction of the orthotropic plate ($c_T = 1080$ m/s). At this velocity, a_1 will appear when $f \cdot h$ reaches approximately 0.54 MHz. This $f \cdot h$ value was not reached during testing, implying that the second order flexural plate wave was most likely *not* present, leaving only the lowest order plate modes.

Dispersion curves

Dispersion curves were constructed for all panels by measuring phase velocity for differ-

ent $f \cdot h$ products (Fig. 11). For the orthotropic plate, a dispersion curve was constructed for each in-plane principal material direction.

Dispersion curves from 3.2-mm and 6.4-mm transversely isotropic plates follow the same path, as can be seen in Fig. 11; however, they possess markedly different flexural rigidities. This validates the ability to normalize dispersion curves relative to thickness for wood composite plates.

Neither the individual fibers nor the laminations appeared to influence the plate wave propagation, but instead the panels were "perceived" as single homogeneous sheets of material. Based on the linear relationship of relative RX distance to phase point transit time (Fig. 7), all fabricated panels exhibited relative material homogeneity in the NDE test region (center of the panel). Phase velocities were plotted (Fig. 11) until erratic signals prevented the accurate location of phase points due to the reduced sensitivity of the transducer at smaller wavelengths (Huang 1998).

When the dispersion curves from the 6.4-mm laminated and the 6.4-mm solid transversely isotropic panels (Fig. 11) were compared, only slight differences were observed, indicating that plate waves behave similarly in both solid and laminated panels made of the same material. The plate wave technique indicated slightly higher flexural and transverse shear rigidities (12% and 25%, respectively) for the laminated specimen (Fig. 12); however, these higher rigidities were verified (in the following sections) by mechanical testing and normal contact ultrasonic shear wave speed. Thus, the higher laminate rigidities were due to the actual panel properties and *not* a limitation of the plate wave technique.

Comparing the two in-plane principal material directions of the orthotropic plate revealed largely different dispersion curves (Fig. 11), indicating that the direction perpendicular to the fiber orientation (2-direction) possessed much lower material rigidities than the direction parallel to the fiber orientation (1-direction). Since the 1- and 2-direction dispersion curves approached a constant phase velocity
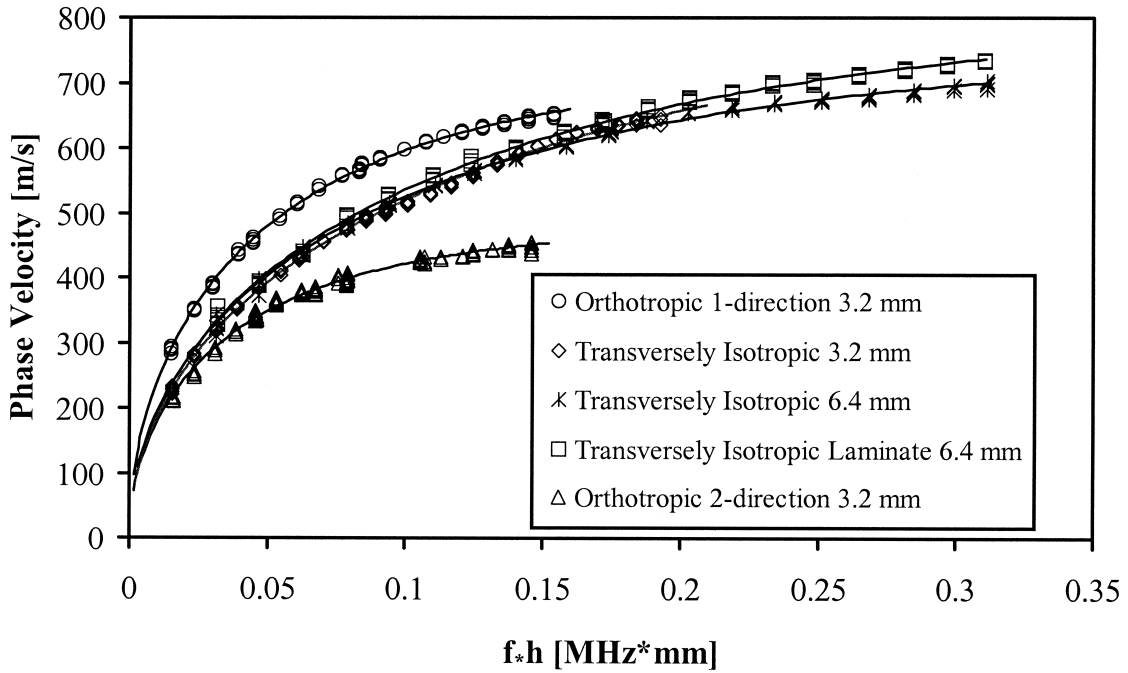
FIG. 11. Dispersion curves indicating phase velocity for various $f \cdot h$ values: curves presented for 3.2 mm, 6.4 mm, and laminated transversely isotropic fiberboard plates closely follow the same trend; large material differences were observed in the two in-plane, principal material directions of the orthotropic plates.

at approximately 660 and 450 m/s, respectively, the plate possessed a lower shear modulus in the 2-3 plane than in the 1-3 plane. In addition, the 1-direction dispersion curve had a higher initial slope than the 2-direction curve, indicating a higher flexural rigidity for bending about the 2-axis than for the 1-axis.

Considering the 3.2-mm solid, 6.4-mm sol-

FIG. 12. Comparison of flexural rigidity values obtained from plate wave and mechanical bending tests.

id, and 6.4-mm laminated transversely isotropic plates, extensional phase velocities were approximately equal, implying that extensional phase velocity was indeed independent of thickness and laminations at low frequencies. Extensional phase velocities obtained from the orthotropic plate indicated a "preferred" orientation (similar to the flexural results) with the 1-direction velocity being approximately two times greater than the 2-direction, implying a higher 1-direction axial rigidity.
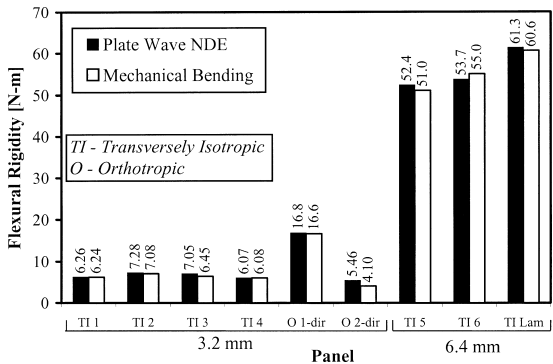
Flexural plate rigidity

Flexural rigidity values obtained from the plate wave technique were compared with values obtained from mechanical bending tests and found to be in excellent agreement (Fig. 12). Values for the flexural rigidity were within 3% for most plates, except for the 2-direction of the orthotropic plate with a 33% difference relative to the mechanical test results. Much higher rigidity values were found (and
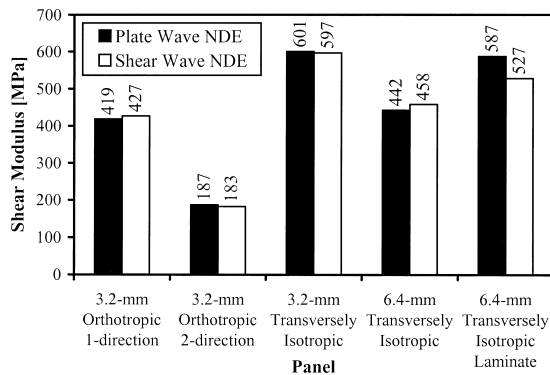
FIG. 13.   Comparison of transverse shear rigidity values obtained from plate wave technique and normal contact through-thickness ultrasonic bulk shear wave testing.
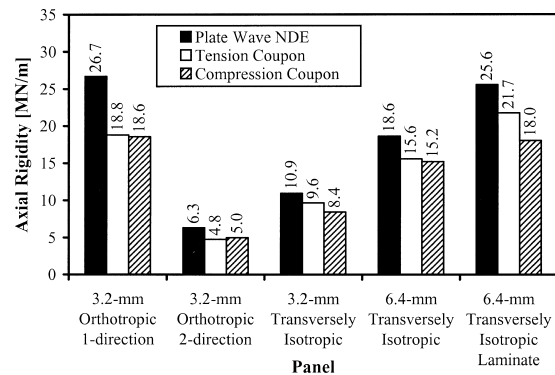

FIG. 14.   Comparison of plate wave and axial mechanical coupon results: plate wave results could be higher due to load-rate effects and/or differences in stress states.

anticipated) for thicker panels since the rigidity is a cubic function of thickness. As previously stated, solid and laminated transversely isotropic plates of the same thickness exhibited similar rigidities. Both plate wave and mechanical testing indicated that the flexural rigidity of the orthotropic plate in the 1-direction was three times greater than in the 2-direction and more than two times greater than the transversely isotropic plates of the same thickness. Overall, the plate wave technique accurately measured the flexural plate rigidities of the panels tested herein.

Transverse shear plate rigidity

Good agreement for transverse shear moduli was observed between plate wave and through-thickness ultrasonic testing (Fig. 13). Shear modulus, G_{13} or G_{23}, was calculated from transverse shear rigidity, A_{55} or A_{44}, assuming a shear correction factor for a rectangular cross section ($K = 0.833$) (Tang et al. 1988). Most results agreed within 3.4% except for the transversely isotropic laminate results that differed by 11.4%. Differences could be due to the fact that through-thickness measurement locations on the panels were not coincident with plate wave measurement locations. Additional measurements of phase velocity obtained at higher $f \cdot h$ values (above those obtained in this study) could provide even better plate wave results by providing a

more complete dispersion curve. However, due to equipment limitations, degradation in signal quality prevented accurate phase velocity measurements at higher frequencies.

Axial plate rigidity

Comparisons of axial rigidity obtained from mechanical coupon testing and plate wave testing are presented in Fig. 14. As can be seen, axial stiffness values obtained from NDE were notably higher (between 12% and 31%) than those obtained from mechanical tension testing. Discrepancies between tensile and compressive rigidity could be due to dissimilar compressive and tensile moduli (Meyers 2001). However, this offers no explanation for the variation between plate wave and mechanical coupon tests, which could be due to a combination of reasons including differing stress states and load-rate effects.

One possible inconsistency between plate and coupon tests was the change in boundary conditions on the material. When the coupons were removed from the plate, the boundary conditions were altered, thus violating the plane stress plate wave assumption. During testing of the coupons, a unidirectional state of stress was created when freed from surrounding material. Assuming a Poisson's ratio to calculate axial coupon rigidity per unit width, AE/w (A is area, E is elastic modulus, and w is width), the mechanical coupon values

may be compared to the plate wave values for axial rigidity, A_{11} or A_{22}. A range of values for Poisson's ratio was explored, but only small improvements in agreement between NDE and mechanical testing were observed. These were not enough to account for the entire difference between plate wave NDE and axial tests.

Another possible reason for variation between plate wave and mechanical test results is the large difference in load rate between the tests (Halabe et al. 1997). Mechanical loading of the coupon specimens was performed with a strain rate of 1.0% per minute, whereas extensional plate waves load and unload the material more than a million times faster. Since natural fibers are viscoelastic, increased loading rate results in increased values of Young's modulus. This behavior has been witnessed using stress wave speed as an indicator for Young's modulus in lumber. If the exact load-rate effect were known for each specimen, correction factors could be applied. It is interesting to note that the speculated load-rate effect was not apparent in the flexural rigidity comparisons.

CONCLUSIONS AND RECOMMENDATIONS

An NDE procedure was developed for using plate waves to determine material properties in natural fiber composite plates up to 6.4-mm thick. The experimental setup was verified using a 6061-T4 aluminum alloy plate. Based on the results of this research, the evaluation of flexural, axial, and transverse shear rigidity for thin (less than 6.4 mm thick) natural fiber-based panels was shown to be technically feasible.

Comparison of flexural rigidity obtained from plate wave and mechanical tests revealed only a 3% variation, except for the 2-direction of the orthotropic plate with a 33% difference. Transverse shear moduli obtained from plate wave tests were within 3% of through-thickness ultrasonic tests, except for the laminate with an 11% difference.

Axial rigidity values obtained from plate wave testing were between 12% and 31% higher than values obtained from tensile cou-

pon tests and between 22% and 41% greater than compressive coupon values. Past wood research has also noted these higher modulus values obtained from NDE due to load rate effects. However, this speculated load-rate phenomenon was not observed for the flexural rigidity values.

This research examined panels up to 6.4 mm (0.25 in.) in thickness. Due to the low frequencies and long wavelengths, neither the individual fibers nor the laminations appeared to influence the plate wave propagation. Instead, the panels were "perceived" as single homogeneous sheets of material. Thicker panels could be tested with this same technique; however, there are testing guidelines and limitations that should be addressed. With a thicker panel the ultrasonic signal is attenuated faster, likely due to the increased rotational inertia effects, giving rise to higher dissipation of the plate wave energy. To stay within the limits for plate wave propagation and achieve sufficient dispersion curve resolution, low frequencies and smaller frequency increments must be used. At higher $f{\cdot}h$ values (depending on material properties) the plate wave assumption is no longer valid and additional Lamb wave modes begin to propagate (e.g., the next highest Lamb mode, a_1, would appear at an $f{\cdot}h$ ratio of approximately 0.4 for the panels tested herein). These higher order Lamb wave modes could be used to extract more information about the material. However, the additional information requires more advanced experimental setup, signal processing, and data analysis.

It was found that a larger transducer diameter (face area) had an adverse effect on the received signal details. One method of minimizing this error is to measure plate displacement at a single point using a device such as a laser interferometer, possibly resulting in cleaner, more discernible signals at higher $f{\cdot}h$ values above those attained in this research. This type of setup would be advantageous, if not essential, for discerning higher Lamb wave modes.

While this research used direct normal contact with the specimen to determine the technical feasibility of the plate wave method, fu-

ture research should focus on non-contact determination of panel rigidity for on-line applications. Also note that through-thickness shear wave testing (used to verify the plate wave testing results) requires the use of high viscosity couplant in direct contact with the specimen. Thus, while determination of G using normal-contact, through-thickness shear wave testing was useful in these laboratory tests, it is not feasible for in-line panel NDE.

Future research should also focus on signal processing issues. Wavelet transforms and the Fast Fourier Transform phase spectra could be used to determine wave speeds of different frequencies in a broadband (multi-frequency) pulse. This would eliminate the need for discrete excitation of frequencies and the tedious signal processing techniques used in this research.

REFERENCES

AMERICAN SOCIETY FOR TESTING AND MATERIALS (ASTM). 1996. Standard test method for compressive properties of rigid plastics. ASTM D 695-96. ASTM, West Conshohocken, PA.

⸻. 2000. Standard test method for tensile properties of plastics. ASTM D 638-00. ASTM, West Conshohocken, PA.

AULD, B. A. 1973. Acoustic fields and waves in solids, vol. II. John Wiley & Sons, Inc. New York, NY.

BEALL, F. C. 1990. Use of AE/AU for evaluation of adhesively bonded wood base materials. *In* Proc. 7th Symposium on Nondestructive Testing of Wood, September 27–29, 1989, Madison, WI.

⸻, AND J. M. BIERNACKI. 1992. An approach to the evaluation of glulam beams through acousto-ultrasonics. *In* Proc. 8th Symposium on Nondestructive Testing of Wood, September 23–25, 1991, Vancouver, WA.

⸻, AND L. CHEN. 1997. Ultrasonic monitoring of resin curing in a laboratory press. Proc. Workshop on Nondestructive Testing of Panel Products, Wales, UK.

BRASHAW, B. K., R. J. ROSS, AND R. F. PELLERIN. 1996. Stress wave nondestructive evaluation of green veneer: Southern yellow pine and Douglas-fir. *In* S. Doctor, C. A. Lebowitz, and G. Y. Baaklini, eds. Nondestructive evaluation of materials and composites. The International Society for Optical Engineering, Bellingham, WA.

BRAY, D. E., AND R. K. STANLEY. 1997. Nondestructive evaluation: A tool in design, manufacturing, and service. CRC Press, New York, NY.

ENSMINGER, D. 1988. Ultrasonics 2/E. Marcel Dekker, Inc., New York, NY.

GRAFF, K. F. 1975. Wave motion in elastic solids. Ohio State University Press, Columbus, OH.

HALABE, U. B., G. M. BIDIGALU, H. V. S. GANGARAO, AND R. J. ROSS. 1997. Nondestructive evaluation of green wood using stress wave and transverse vibration techniques. Materials Eval. 55(9):1013–1018.

HUANG, W. 1998. Application of Mindlin plate theory to analysis of acoustic emission waveforms in finite plates. *In* D. O. Thompson and D. E. Chimenti, eds. Proc. 24th Annual Symposium on Quantitative Nondestructive Evaluation, July 27–August 1, 1997, San Diego, CA.

⸻. 1999. Verbal communication. Digital Wave Corporation, Englewood, CO.

⸻, S. M. ZIOLA, J. F. DORIGHI, AND M. R. GORMAN. 1998. Stiffness measurement and defect detection in laminated composites by dry-coupled plate waves. *In* R. H. Bossi and D. M. Pepper, eds. Proceedings of SPIE, March 31–April 2, San Antonio, TX.

MEYERS, K. L. 2001. Effect of strand geometry and orientation on wood composites. M.S. thesis, Department of Civil and Environmental Engineering, Washington State University, Pullman, WA.

MINDLIN, R. D. 1951. Influence of rotatory inertia and shear on flexural motions of isotropic, elastic plates. J. Appl. Physics 18:31–38.

PETIT, M. H., V. BUCUR, AND C. VIRIOT. 1992. Aging monitoring of structural flakeboards by ultrasound. *In* Proc. 8th Symposium on Nondestructive Testing of Wood, September 23–25, 1991, Vancouver, WA.

ROSE, W. R. 1999. Ultrasonic waves in solid media. Cambridge University Press, Cambridge, UK.

ROSS, R. J. 1999. Using sound to evaluate standing timber. Int. Forestry Rev. 1(1):43–44.

⸻, AND R. F. PELLERIN. 1988. NDE of wood-based composites with longitudinal stress waves. Forest Prod. J. 38(5):39–45.

⸻, ⸻, N. VOLNY, W. W. SALSIG, AND R. H. FALK. 1999. Inspection of timber bridges using stress wave timing nondestructive evaluation tools. General Technical Report FPL-GTR-114. USDA Forest Prod. Lab., Madison, WI.

SATO, K., AND M. FUSHITANI. 1992. Development of nondestructive testing system for wood-based materials utilizing acoustic emission technique. *In* Proc. 8th Symposium on Nondestructive Testing of Wood, September 23–25, 1991, Vancouver, WA.

SEALE, M. D., AND E. I. MADARAS. 2000. Transducer effects in ultrasonic measurements of material stiffness. Exp. Techniques 24(6):35–38.

STIFFLER, R. C. 1986. Wave propagation in composite plates. Ph.D. dissertation, College of Engineering, Virginia Polytechnic Institute and State University, Blacksburg, VA.

TANG, B., AND E. G. HENNEKE II. 1989. Long wavelength approximation for Lamb wave characterization of composites laminates. Res. in Nondestr. Eval. 1:51–64.

⸻, ⸻, AND R. C. STIFFLER. 1988. Low frequency flexural wave propagation in laminated composite plates. Pages 45–65 *in* J. C. Duke, Jr., ed., Acousto-

ultrasonics: Theory and application. Plenum Press, New York, NY.

TAUCHERT, T. R., AND A. N. GUZELSU. 1972. An experimental study of dispersion of stress waves in a fiber-reinforced composite. J. Appl. Mech. 39(3):98–102.

TUCKER, B. J. 2001. Ultrasonic plate waves in wood-based composite panels. Ph.D. dissertation, Washington State University, Pullman, WA.

VIKTOROV, I. A. 1967. Rayleigh and Lamb waves: Physical theory and applications. Plenum Press, New York, NY.